High-resolution FEM-TVD schemes based on a fully multidimensional flux limiter

D. Kuzmin* and S. Turek

Institute of Applied Mathematics (LS III), University of Dortmund
Vogelpothsweg 87, D-44227, Dortmund, Germany

Abstract

A new approach to the derivation of local extremum diminishing finite element schemes is presented. The monotonicity of an arbitrary Galerkin discretization is enforced by adding discrete diffusion so as to eliminate negative off-diagonal matrix entries. The resulting low-order operator of upwind type acts as a preconditioner within a nonlinear defect correction loop. A multidimensional generalization of TVD concepts is employed to design solution-dependent antidiffusive fluxes which are inserted into the defect vector in order to preclude excessive smearing by numerical diffusion. Standard one-dimensional limiters can be applied edge-by-edge so as to control the slope ratio for the three-point stencil which is reconstructed using a special positivity-preserving gradient recovery. In this paper, a superior limiting strategy is introduced which consists in balancing the diffusive and antidiffusive contributions to each node and applying the resulting correction factors to the incoming antidiffusive fluxes. The proposed algorithm can be readily incorporated into existing flow solvers as a 'black-box' postprocessing tool for the matrix assembly routine. Its performance is illustrated by a number of numerical examples for scalar convection problems and incompressible flows in two and three dimensions.

Key Words: convection-dominated problems; high-resolution schemes; flux limiters; finite elements; unstructured grids

1 Introduction

An adequate treatment of unstable convective terms is a matter of utmost importance for the majority of CFD applications. Solutions produced by standard discretization techniques are typically corrupted by nonphysical oscillations and/or excessive numerical diffusion. Traditionally, these problems have been dealt with by means of a nonlinear shock-capturing viscosity. Modern high-resolution schemes are based on flux/slope limiters which switch between linear high- and low-order discretizations adaptively depending on the smoothness of the solution. The foundations of this methodology were laid by Boris and Book [2] who introduced the pioneering concept of flux-corrected-transport (FCT). A genuinely multidimensional generalization of the original FCT algorithm was proposed by Zalesak [39] and carried over to finite elements by Löhner *et al.* [24],[25].

*Correspondence to: kuzmin@math.uni-dortmund.de

In a series of recent publications [14],[15],[16],[17] we extended the classical FEM-FCT formulation to implicit time-stepping and developed a coherent theory for the design of positivity-preserving schemes on arbitrary meshes. In this paper, we employ similar tools to investigate and promote another important class of high-resolution schemes which was established by Harten [8],[9]. His total variation diminishing (TVD) methods and extensions thereof rest on a firm mathematical basis and have enjoyed an increasing popularity over the past two decades. However, both the theory and the algorithms are essentially one-dimensional and no rigorous generalization to the multidimensional case is available to date. As a matter of fact, most of the CFD codes utilizing a (quasi-) TVD discretization of convective terms resort to directional splitting on Cartesian grids.

In light of the above, TVD limiters have hardly been used in the finite element context. In scarce publications on that subject, TVD-like artificial viscosities were designed using an *ad hoc* reconstruction of local one-dimensional stencils associated with edges of the finite element mesh [1],[26],[27]. Even though the numerical results were found to be quite promising, such schemes cannot be guaranteed to be positivity-preserving and may fail to suppress the nonphysical oscillations in some cases. Moreover, the use of simplex elements with a piecewise-linear approximation is essential to the derivation of the underlying edge-based data structure as proposed by Peraire *et al.* [30]. Therefore, this approach is not suitable for multilinear and higher order finite elements and rules out the conventional implementation of a flow solver with an element-by-element matrix assembly.

Below we demonstrate that arbitrary Galerkin discretizations with a finite element interpolation of the flux function admit a conservative decomposition into skew-symmetric numerical fluxes between individual nodes. In the case of P_1-elements, these fluxes can indeed be associated with the actual mesh edges. In general, two neighboring nodes may engage in a bilateral mass exchange if their basis functions have overlapping supports. The transition to a suitable 'edge-based' data structure may reduce the overhead incurred by indirect addressing and offer considerable savings in terms of both CPU time and memory requirements [23],[26]. At the same time, this kind of data structure is not mandatory, unlike in the edge-oriented FEM-TVD method of Lyra *et al.* [27]. As we are about to see, it suffices to represent the (anti-)diffusive terms as an array of internodal fluxes which can be constructed and limited edge-by-edge in a mass-conserving fashion.

The novel approach pursued in this paper distinguishes itself in that it is applied at the fully discrete level and operates with finite element matrices regardless of the underlying mesh, approximation spaces and even the number of spatial dimensions. It amounts to modifying the discrete transport operators so as to enforce the M-matrix property and render the discretization local extremum diminishing. To this end, the oscillatory high-order operator is transformed into a monotone low-order one by a conservative elimination of negative off-diagonal entries [15]. This technique resembles classical upwinding and leads to a new interpretation of TVD concepts which remains valid in multidimensions.

To recover the high accuracy of the original discretization in regions where the solution is sufficiently smooth, excessive numerical diffusion is removed by adding nonlinear compensating antidiffusion. The formation of wiggles is precluded by a flux limiter which controls the slope ratio in the direction of the numerical edge or the net antidiffusive contribution to each node. In either case, the discretization is proved to be positivity-preserving. The first method (slope-limiter TVD) represents a generalization of the stan-

dard approach based on an edgewise stencil reconstruction. The second one (flux-limiter TVD) is conceptually different and utilizes some features of the multidimensional FCT formulation. It turns out to be more robust and exhibits much better convergence rates to the steady state, at least in the case of certain nonconforming finite elements which lend themselves to the numerical treatment of the incompressible Navier-Stokes equations. Moreover, no *ad hoc* recovery of solution values at fictitious 'dummy nodes' is necessary, so that the limiter is completely independent of the mesh topology. All the required information is inferred from the coefficients and the sparsity pattern of the discrete operators. This new FEM-TVD methodology constitutes the main highlight of this paper.

2 One-dimensional TVD schemes

Let us briefly review the classical TVD methodology in order to introduce some basic concepts and identify the main difficulties which hinder a genuinely multidimensional generalization. A detailed presentation of this material can be found in [10],[21],[36].

It is well known that any physically admissible solution to a scalar conservation law

$$\frac{\partial u}{\partial t} + \frac{\partial f}{\partial x} = 0, \tag{1}$$

where f is a flux function, is characterized by a nonincreasing total variation defined as

$$TV = \int \left| \frac{\partial u}{\partial x} \right| \, dx. \tag{2}$$

Thus, it is natural to impose the same constraint on the numerical solution, so that

$$TV(u^{n+1}) \leq TV(u^n), \qquad \text{where} \quad TV(u) = \sum_i |u_{i+1} - u_i|. \tag{3}$$

Harten [8] proved that a conservative semi-discrete difference scheme

$$\frac{du_i}{dt} + \frac{f_{i+1/2} - f_{i-1/2}}{\Delta x} = 0 \tag{4}$$

is total variation diminishing provided that it can be rewritten in the form

$$\frac{du_i}{dt} = c_{i-1/2}(u_{i-1} - u_i) + c_{i+1/2}(u_{i+1} - u_i) \tag{5}$$

with (possibly nonlinear) nonnegative coefficients $c_{i-1/2} \geq 0$ and $c_{i+1/2} \geq 0$. Furthermore, an additional CFL-like condition must be reckoned with unless the fully implicit backward Euler method is employed for the time discretization [8],[15].

According to the Godunov theorem [6], linear TVD schemes are doomed to be at most first-order accurate. To circumvent this serious limitation, the numerical fluxes $f_{i\pm1/2}$ can be constructed in a nonlinear way by blending high- and low-order approximations

$$f_{i\pm1/2} = f^L_{i\pm1/2} + \Phi_{i\pm1/2}[f^H_{i\pm1/2} - f^L_{i\pm1/2}]. \tag{6}$$

Here $\Phi_{i\pm1/2}$ is an adaptive correction factor which is referred to as the *flux limiter* and designed so as to satisfy Harten's TVD conditions. As a rule of thumb, it should be set equal to zero in the vicinity of steep gradients and may take values up to 2 in regions where the solution is smooth. This corresponds to adding a proper amount of nonlinear *antidiffusion* to the low-order flux approximation $f^L_{i\pm1/2}$ so as to improve the accuracy without generating spurious wiggles and violating the TVD property.

To elucidate the ins and outs of this hybrid method in a rather simple setting, let us consider the linear convection equation

$$\frac{\partial u}{\partial t} + v\frac{\partial u}{\partial x} = 0 \tag{7}$$

with a constant velocity $v > 0$. In the course of space discretization, the underlying flux function $f(u) = vu$ is typically approximated by

$$f^L_{i+1/2} = vu_i \qquad \text{upwind difference method} \tag{8}$$

or

$$f^H_{i+1/2} = v\frac{u_{i+1} + u_i}{2} \qquad \text{central difference method.} \tag{9}$$

The incoming fluxes $f^L_{i-1/2}$ and $f^H_{i-1/2}$ are defined simply by shifting the index i. It can be easily verified that the upwind-biased flux approximation yields a first-order accurate (linear) TVD scheme with the coefficients $c_{i-1/2} = v/\Delta x$, $c_{i+1/2} = 0$. To recover the second-order accuracy of the central difference discretization whenever possible, we insert the above approximations into (6) to obtain the nonlinear TVD flux

$$f_{i+1/2} = vu_i + \frac{v}{2}\Phi_{i+1/2}(u_{i+1} - u_i). \tag{10}$$

To determine the magnitude of admissible antidiffusive correction, the flux limiter Φ must examine the local smoothness of the solution. A suitable sensor is provided by the ratio of consecutive gradients evaluated at the grid point located upwind. In the case of a positive velocity, we have $\Phi_{i+1/2} = \Phi(r_i)$. The involved slope ratio

$$r_i = \frac{u_i - u_{i-1}}{u_{i+1} - u_i} \tag{11}$$

is obviously negative at a local extremum (see Figure 1), close to unity for smooth data and large if the numerical solution tends to change abruptly.

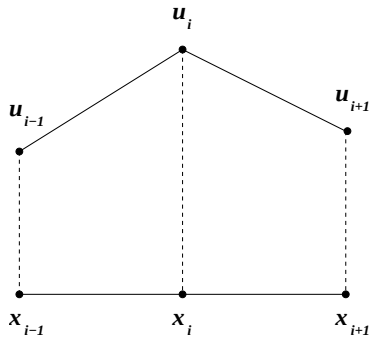

Figure 1. Three-point stencil in one dimension.

As shown by Jameson [11], it is worthwhile to interpret and implement the flux limiter Φ in terms of a special limited average operator $\mathcal{L}$ being a function of two variables such that $\Phi(r) = \mathcal{L}(1, r)$. This operator is supposed to possess the following properties:

P1. $\mathcal{L}(a, b) = \mathcal{L}(b, a)$.

P2. $\mathcal{L}(ca, cb) = c\mathcal{L}(a, b)$.

P3. $\mathcal{L}(a, a) = a$.

P4. $\mathcal{L}(a, b) = 0 \quad \text{if } ab \le 0$.

In particular, the last property ensures that $\Phi(r) = 0$ if $r \le 0$ and $\Phi(r) > 0$ otherwise. Thus, the accuracy of a TVD discretization inevitably degrades to first order at local extrema. Another important implication is the symmetry of the flux limiter

$$\Phi(r) = \mathcal{L}(1, r) = r\mathcal{L}(1/r, 1) = r\Phi(1/r) \tag{12}$$

which follows from the properties (P1) and (P2). By virtue of this identity, the antidiffusive flux received by the grid point i from its right neighbor is given by

$$\Phi(r_i)(u_{i+1} - u_i) = \mathcal{L}(u_{i+1} - u_i, u_i - u_{i-1}) = \Phi(1/r_i)(u_i - u_{i-1}) \tag{13}$$

and has the same effect as a diffusive flux from the left neighbor if $\Phi(1/r_i) > 0$. Note that working with $\mathcal{L}$ rather than Φ prevents division by zero in the denominator of r_i.

Making use of the definition (11), one can represent the semi-discrete scheme for the convection equation in the desired form (5) with the coefficients

$$c_{i-1/2} = \frac{v}{2\Delta x}\left[2 + \frac{\Phi(r_i)}{r_i} - \Phi(r_{i-1})\right], \qquad c_{i+1/2} = 0. \tag{14}$$

To meet the requirements of Harten's theorem, the expression in the brackets must be nonnegative. A variety of limiters designed to enforce this condition have been proposed in the literature. Some of the most popular two-parameter ones are as follows

$$\begin{aligned}
&\text{minmod:} && \mathcal{L}(a, b) = \mathcal{S}(a, b) \cdot \min\{|a|, |b|\}, \\
&\text{Van Leer:} && \mathcal{L}(a, b) = \mathcal{S}(a, b) \cdot \frac{2|a||b|}{|a|+|b|}, \\
&\text{2-mean:} && \mathcal{L}(a, b) = \mathcal{S}(a, b) \cdot \min\left\{\frac{|a+b|}{2}, 2|a|, 2|b|\right\}, \\
&\text{superbee:} && \mathcal{L}(a, b) = \mathcal{S}(a, b) \cdot \max\{\min\{2|a|, |b|\}, \min\{|a|, 2|b|\}\}.
\end{aligned}$$

Here $\mathcal{S}(a, b)$ stands for the synchronized sign function

$$\mathcal{S}(a, b) = \frac{\text{sign}(a) + \text{sign}(b)}{2} = \begin{cases} 1 & \text{if } a > 0 \ \wedge \ b > 0, \\ -1 & \text{if } a < 0 \ \wedge \ b < 0, \\ 0 & \text{otherwise.} \end{cases}$$

The associated one-parameter limiters Φ yield correction factors lying in the range $[0, 2]$. Note that the integer values $0, 1, 2$ result in the standard upwind, central and downwind approximation, respectively.

Nowadays, TVD schemes of this kind are widely used in CFD software in conjunction with finite difference and finite volume discretizations on structured grids. At the same time, a finite element practitioner considering the implementation of the above algorithm in a general purpose code is faced by (at least) the following challenges:

- how to cast a finite element scheme in conservation form?
- how to generalize Harten's TVD criteria to multidimensions?
- how to perform upwinding in the finite element context?
- how to deal with variable mesh size and/or velocity field?
- how to discretize nonlinear source and/or sink terms?
- how to define the parameter r_i on unstructured grids?
- how to treat nonlinear problems in an implicit way?

These problems proved to be a rather hard nut to crack, so that the development of FEM-TVD methods has eventually ended up in a deadlock. In what follows, we will give answers to the questions listed above and propose a new methodology for the design of TVD-type finite element discretizations on unstructured grids.

3 Galerkin flux decomposition

The first issue to be clarified is the representation of a finite element scheme in conservation form such as (4). In contrast to finite difference and finite volume methods, the Galerkin FEM is based on a weak formulation which is conservative in an integral sense [7] but does not admit a natural decomposition into a sum of *numerical fluxes* from one node into another. Since most high-resolution schemes operate with such fluxes, their extension to finite elements proved to be a formidable task. Peraire *et al.* [30] were the first to demonstrate that a conservative flux decomposition is feasible for the Galerkin method employing triangular or tetrahedral elements with linear basis functions. The authors advocated the transition to an edge-based data structure which offers certain computational advantages as compared to the conventional element-based formulation. Moreover, it yields a general framework for implementation of many essentially one-dimensional high-resolution schemes (including those of TVD type) on unstructured meshes in conjunction with a finite element discretization. The interested reader is referred to the monographs by Lyra [26] and Löhner [23] for a detailed presentation of this approach.

The above-mentioned data structure due to Peraire *et al.* was utilized in a number of state-of-the-art finite element algorithms for numerical simulation of compressible flow problems on unstructured grids. A comprehensive review of such edge-based FEM solvers

is available in the recent article by Morgan and Peraire [28]. Unfortunately, the underlying flux decomposition is only valid for simplex elements with linear interpolation of the unknown solution and of the associated flux function [23]. Below we present an alternative formulation applicable to general finite element approximations on arbitrary meshes including quadrilateral and hexahedral ones [16].

Consider a generic time-dependent conservation law for a scalar quantity u

$$\frac{\partial u}{\partial t} + \nabla \cdot \mathbf{f} = q \qquad \text{in } \Omega, \tag{15}$$

where q is a source term and $\mathbf{f}$ is a flux function which may depend on the solution in a nonlinear way. As a rule, we can distinguish between convective fluxes of the form $\mathbf{f}_c = \mathbf{v}u$ and diffusive fluxes of the form $\mathbf{f}_d = -\epsilon \nabla u$.

Using the divergence theorem to integrate the spatial derivatives in the weak form of equation (15) by parts, we obtain

$$\int_\Omega w \frac{\partial u}{\partial t}\, d\mathbf{x} - \int_\Omega \nabla w \cdot \mathbf{f}\, d\mathbf{x} + \int_{\partial\Omega} w\ \mathbf{f} \cdot \mathbf{n}\ ds - \int_\Omega wq\, d\mathbf{x} = 0, \qquad \forall w. \tag{16}$$

A common practice in finite element methods for conservation laws is to interpolate the fluxes and source terms in the same way as the numerical solution

$$u = \sum_j u_j \varphi_j, \qquad \mathbf{f} = \sum_j \mathbf{f}_j\, \varphi_j, \qquad q = \sum_j q_j \varphi_j, \tag{17}$$

where φ_i denote the basis functions spanning the finite-dimensional subspace. This kind of approximation was called the *group finite element formulation* by Fletcher [5] who found it to provide a very efficient treatment of nonlinear convective terms and even lead to a small gain of accuracy for the 2D Burgers equation discretized on a uniform grid.

The resulting Galerkin discretization of equation (15) reads

$$\sum_j \left[\int_\Omega \varphi_i \varphi_j\, d\mathbf{x} \right] (\dot{u}_j - q_j) - \sum_j \left[\int_\Omega \nabla \varphi_i \varphi_j\, d\mathbf{x} - \int_{\partial\Omega} \varphi_i \varphi_j\, \mathbf{n}\ ds \right] \cdot \mathbf{f}_j = 0. \tag{18}$$

Note that for most finite elements the sum of basis functions equals unity: $\sum_i \varphi_i \equiv 1$. Summing the semi-discretized equations over i, one recovers the integral form of the conservation law, which ensures that the total amount of u in Ω may only change due to boundary fluxes and internal sources or sinks. Thus, the Galerkin method does possess the global conservation property. Our objective is to show that the volume integrals

$$\delta u_i = \sum_j \mathbf{c}_{ij} \cdot \mathbf{f}_j, \qquad \text{where} \quad \mathbf{c}_{ij} = \int_\Omega \nabla \varphi_i\, \varphi_j\, d\mathbf{x}, \tag{19}$$

admit a decomposition into skew-symmetric numerical fluxes resembling their finite difference and finite volume counterparts.

Since the basis functions sum to unity, the sum of their derivatives vanishes. Hence, the coefficient matrices $\mathbf{c}_{ij}$ are characterized by having zero column sums, which enables us to express their diagonal entries in terms of the off-diagonal ones

$$\sum_i \mathbf{c}_{ij} = 0 \quad \Rightarrow \quad \mathbf{c}_{ii} = -\sum_{j \neq i} \mathbf{c}_{ji}. \tag{20}$$

It follows that the interior part of the discretized flux term can be rewritten as

$$\delta u_i = \sum_{j \neq i} f_{ij}, \qquad \text{where} \quad f_{ij} := \mathbf{c}_{ij} \cdot \mathbf{f}_j - \mathbf{c}_{ji} \cdot \mathbf{f}_i. \tag{21}$$

The so defined quantity f_{ij} can be interpreted as a 'projection' of the averaged flux onto the segment joining the interacting nodes. Therefore, it will be called the *Galerkin flux* from node j into node i. In one dimension, the weighting coefficients for a piecewise-linear finite element discretization on a uniform mesh are given by $c_{ij} = -c_{ji} = 1/2$, so that $f_{ij} = (f_i + f_j)/2$. This is due to the well-known fact that the Galerkin method results in a central difference type approximation of differential operators.

Unlike the algorithm of Peraire *et al.* [30], the above flux decomposition is rather straightforward and valid for a wide range of finite element discretizations. Our Galerkin fluxes are associated with edges of the graph representing the sparsity pattern of the finite element matrix rather than the topology of the underlying computational mesh. For linear triangles or tetrahedra, this distinction makes no difference, whereas multilinear or high-order FEM approximations give rise to some edges of purely artificial origin. In general, local degrees of freedom may interact by exchanging mass and other conserved quantities on a bilateral basis. By definition (21), the corresponding fluxes are skew-symmetric, i.e. $f_{ji} = -f_{ij}$ for any pair of neighboring nodes i and j. Therefore, the numerical scheme is guaranteed to satisfy the discrete conservation principle.

A promising approach to the derivation of nonoscillatory finite element methods consists in replacing the Galerkin flux by another consistent numerical flux. Its potential was demonstrated by numerous publications in which popular upwind-biased schemes and their high-resolution extensions based on one-dimensional flux limiters were successfully applied on unstructured meshes in conjunction with the edge-based data structure [23], [26], [28]. In particular, Lyra *et al.* [27] designed TVD-like artificial viscosities by insertion of two dummy nodes so as to reconstruct a local one-dimensional stencil and generate a numerical flux of the form (10) for each edge. The required solution values at the dummy nodes were evaluated using the finite element shape functions or a variational gradient recovery by means of an L_2-projection (see below). Simulation results were reported to be encouraging but rather sensitive to the choice of the reconstruction procedure, especially in the case of highly irregular meshes [26].

Our flux decomposition strategy makes it possible to apply the wealth of discretization tools developed for the edge-based data structure of Peraire *et al.* [30] in a much more general setting than linear finite elements on triangular meshes. The reader is referred to the monograph [26] for the mathematical and algorithmic background of this approach. In spite of the advantages offered by an edge-based implementation, it might be desirable to integrate TVD limiters into an existing finite element code while preserving the conventional element-oriented data structure. This task can be accomplished by performing flux decomposition just for the involved diffusive/antidiffusive terms. To this end, it is instructive to consider *generalized diffusion operators* which are defined as symmetric matrices having zero row- and column sums [15]

$$D = \{d_{ij}\} \quad \text{such that} \quad \sum_i d_{ij} = \sum_j d_{ij} = 0, \quad d_{ij} = d_{ji}. \tag{22}$$

Note that generalized diffusion operators are not required to have continuous counterparts. Some typical examples are the discrete Laplacian, the streamline-diffusion operator and the artificial diffusion introduced by row-sum mass lumping [15].

A discrete diffusion operator D applied to the vector of nodal values u yields

$$\delta u_i = \sum_j d_{ij} u_j = \sum_{j \neq i} d_{ij}(u_j - u_i) \tag{23}$$

due to the zero row sum. Hence, the following flux decomposition is feasible

$$\delta u_i = \sum_{j \neq i} f_{ij}, \qquad \text{where} \quad f_{ij} = d_{ij}(u_j - u_i). \tag{24}$$

Note that $f_{ji} = -f_{ij}$ due to the symmetry of D. As we will see shortly, these properties of generalized diffusion operators render them a valuable tool for the design of nonoscillatory finite element schemes with and without flux limiters.

4 Discrete upwinding

Recall that classical TVD methods are based on a monotone first-order scheme of upwind type, whose accuracy is enhanced by adding nonlinear antidiffusion to recover a high-order approximation in smooth regions. Unfortunately, it has been largely unclear how to perform upwinding in the finite element framework. Most of the upwind-like finite element methods encountered in the literature resort to a finite volume discretization for the convective terms [1],[38]. An alternative derivation of the least diffusive positivity-preserving scheme can be carried out by adding discrete diffusion depending solely on the magnitude and position of negative matrix entries [14],[15]. In this section, we elucidate the *discrete upwinding* algorithm for a scalar transport equation. A generalization to hyperbolic systems of conservation laws can be found in [17],[19].

Consider the multidimensional convection-diffusion-reaction equation

$$\frac{\partial u}{\partial t} + \nabla \cdot (\mathbf{v} u - \epsilon \nabla u) = q \qquad \text{in } \Omega \tag{25}$$

discretized in space by the lumped-mass Galerkin method without integration by parts. For the sake of efficient matrix assembly, let us employ the group finite element formulation for the convective fluxes and the source terms. The resulting ODE system reads

$$M_L \frac{du}{dt} = Ku + M_L q. \tag{26}$$

Here $M_L = \text{diag}\{m_i\}$ denotes the lumped mass matrix with the entries

$$m_i = \sum_j m_{ij}, \qquad \text{where} \quad m_{ij} = \int_\Omega \varphi_i \varphi_j \, d\mathbf{x}. \tag{27}$$

The discrete transport operator $K = \{k_{ij}\}$ is assembled from [18]

$$k_{ij} = -\mathbf{v}_j \cdot \mathbf{c}_{ji} - \epsilon \, s_{ij}, \tag{28}$$

where $\mathbf{c}_{ji}$ and s_{ij} result from the discretization of differential operators corresponding to the first- and second-order derivatives, respectively

$$\mathbf{c}_{ji} = \int_\Omega \varphi_i \nabla \varphi_j \, d\mathbf{x}, \qquad s_{ij} = \int_\Omega \nabla \varphi_i \cdot \nabla \varphi_j \, d\mathbf{x}. \tag{29}$$

Note that the coefficients m_{ij}, $\mathbf{c}_{ji}$, s_{ij} remain unchanged as long as the mesh is fixed. Therefore, they need to be determined just once during the initialization stage. This enables us to update the matrix K in a very efficient way by computing its entries k_{ij} from formula (28) without resorting to costly numerical integration.

The ODE for each nodal value u_i can be represented in the form

$$m_i \frac{du_i}{dt} = \sum_{j \neq i} k_{ij}(u_j - u_i) + r_i u_i + m_i q_i, \qquad \text{where} \quad r_i = \sum_j k_{ij}. \tag{30}$$

The first term in the right-hand side is engendered by the incompressible part of the discrete transport operator, while $r_i u_i$ is a discrete counterpart of $u \nabla \cdot \mathbf{v}$ which vanishes for divergence-free velocity fields. For the numerical solution to be nonoscillatory even in the vicinity of steep gradients, all off-diagonal coefficients of K must be nonnegative: $k_{ij} \geq 0$, $j \neq i$. This condition is necessary to enforce the M-matrix property and make the discretization *local extremum diminishing* (LED) for incompressible flows in the absence of source terms ($r_i = q_i = 0$). In this case, the semi-discrete scheme reduces to

$$\frac{du_i}{dt} = \sum_{j \neq i} c_{ij}(u_j - u_i), \qquad \text{where} \quad c_{ij} = \frac{k_{ij}}{m_i} \geq 0. \tag{31}$$

Such a discretization proves to be stable in the L_∞-norm. Indeed, if u_i is a maximum, then $u_j - u_i \leq 0$, $\forall j$, so that $\frac{du_i}{dt} \leq 0$. Hence, a maximum cannot increase, and similarly a minimum cannot decrease. As a rule, the coefficient matrices are sparse, so that $k_{ij} = 0$ unless i and j are adjacent nodes. Arguing as above, one can show that a *local* maximum cannot increase, and a *local* minimum cannot decrease.

The above criterion was introduced by Jameson [11],[12],[13] as a handy tool for the design of high-resolution schemes on unstructured meshes. In one dimension, the total variation (3) of the solution can be represented in terms of the local extrema

$$TV(u) = 2\left(\sum \max u - \sum \min u\right). \tag{32}$$

Thus, a one-dimensional LED scheme is necessarily total variation diminishing. At the same time, the LED principle remains valid in multidimensions and is easy to verify.

Any discrete transport operator K can be rendered local extremum diminishing by adding a tensor of artificial diffusion $D = \{d_{ij}\}$ designed so as to eliminate its negative off-diagonal entries. The optimal diffusion coefficients are given by [15],[16]

$$d_{ii} = -\sum_{k \neq i} d_{ik}, \qquad d_{ij} = d_{ji} = \max\{0, -k_{ij}, -k_{ji}\}. \tag{33}$$

By construction, D is a generalized diffusion operator characterized by zero row and column sums. Hence, it entails a redistribution of the conserved quantity u by the diffusive fluxes $f_{ij}^d = d_{ij}(u_j - u_i)$ which reduce the difference between the nodal values.

The elimination of negative matrix entries as proposed above yields the least diffusive LED scheme obtainable from the original Galerkin discretization. For the pure convection equation in one dimension, it is equivalent to the upwind difference method [15],[16]. Note that physical diffusion (if any) built into the coefficients k_{ij} is automatically detected and the amount of artificial diffusion is reduced accordingly. In diffusion-dominated cases, the discrete transport operators K and $L = K + D$ are identical, since the coefficients are nonnegative from the outset. Alternatively, this postprocessing technique can be applied to the convective part of K without taking the physical diffusion into account. This is the approach we adopt in the framework of the FEM-TVD algorithm to be presented.

Discrete upwinding should be performed edge-by-edge in accordance with the sparsity structure of the finite element matrix. Let us start with the Galerkin operator $L = K$. For each pair of neighboring nodes i and j, the required modification is as follows

$$\begin{aligned} l_{ii} &= l_{ii} - d_{ij}, \qquad & l_{ij} &= l_{ij} + d_{ij}, \\ l_{ji} &= l_{ji} + d_{ij}, \qquad & l_{jj} &= l_{jj} - d_{ij}. \end{aligned} \tag{34}$$

In the nontrivial case $d_{ij} = -\min\{k_{ij}, k_{ji}\} > 0$, this amounts to setting either l_{ij} or l_{ji} equal to zero and updating the remaining entries so as to restore the original row/column sums. The row number of the nullified off-diagonal coefficient tells us which of the two nodes is located 'upwind'. Without loss of generality, we assume that i is the *upwind node* for the numerical edge $\vec{ij}$. This edge orientation implies that $l_{ij} = 0$ and $l_{ji} = |k_{ji} - k_{ij}|$. Hence, L can be turned into an upper/lower triangular matrix if convection dominates.

Let us emphasize that the LED constraint is imposed only on the incompressible part of the discrete transport operator K as it should be for physical reasons. The additional term $r_i u_i + m_i q_i$ in the right-hand side of (30) allows for an admissible growth and decay of local extrema due to compressibility and sources/sinks. In order to ensure that the positivity of thermodynamic variables is reproduced by the numerical solution, this term may need to be linearized as proposed by Patankar [29] and explained in our previous publications [16],[17] in the context of positivity-preserving FEM-FCT methods.

5 Iterative defect correction

The modified Galerkin discretization constructed by performing mass lumping and discrete upwinding is optimal in the sense that it introduces just as much artificial diffusion as is necessary to preclude the birth and growth of spurious wiggles regardless of the solution smoothness. Nevertheless, this scheme is linear and therefore at most first-order accurate. To circumvent the restrictive Godunov theorem, a nonoscillatory high-resolution scheme must be nonlinear even for a linear partial differential equation. It is worth mentioning that the majority of practical applications are governed by nonlinear conservation laws to begin with, so that the computational overhead needed to remove excessive artificial diffusion is less significant than in the linear case.

The equations at hand can be discretized in time by the standard θ-scheme. If implicit time-stepping ($0 < \theta \leq 1$) is employed, the nonlinearities inherent to the conservation law and/or to the numerical method must be treated iteratively. Let us update the solution

in each outer iteration using the straightforward defect correction scheme

$$u^{(l+1)} = u^{(l)} + \omega^{(l)}[C(u^{(l)})]^{-1}R(u^{(l)}), \qquad l = 0, 1, 2, \ldots \tag{35}$$

where R is the residual vector and C is a suitably chosen 'preconditioner' which should be easy to invert. The iteration process is terminated when the norm of the defect or that of the relative changes is small enough.

In a practical implementation, the 'inversion' of C is also performed by some iterative procedure. Hence, a certain number of inner iterations per cycle is required to solve the linear subproblem for the solution increment which reads

$$C(u^{(l)})\Delta u^{(l)} = R(u^{(l)}). \tag{36}$$

Afterwards, the weighted correction $\omega^{(l)}\Delta u^{(l)}$ is applied to the last iterate

$$u^{(l+1)} = u^{(l)} + \omega^{(l)}\Delta u^{(l)}, \qquad u^{(0)} = u^n. \tag{37}$$

The underrelaxation factor $\omega^{(l)}$ can be chosen adaptively so as to aid convergence [38]. Note that the auxiliary problem (36) does not have to be solved very accurately at each outer iteration. A moderate improvement of the residual (1-2 digits) is sufficient to obtain a good overall accuracy. The low-order evolution operator

$$C(u^{(l)}) = M_L - \theta\Delta t L(u^{(l)}) \tag{38}$$

constitutes an excellent preconditioner. By construction, C is an M-matrix which makes it amenable to iterative solution. Furthermore, the diagonal dominance of C can be enhanced by using an implicit underrelaxation strategy [4]. It will be noted that defect correction preconditioned by the monotone upwind operator is widely used to enhance the robustness of CFD solvers even in the linear case. This is due to the fact that an iterative method may fail to converge if applied directly to the ill-conditioned matrix originating from a high-order discretization of the bad-behaved convective terms.

The residual vector R for a FEM-TVD scheme is given by

$$\begin{aligned} R(u^{(l)}) &= M_L(u^n - u^{(l)}) + \theta\Delta t[L(u^{(l)}) - A(u^{(l)})]u^{(l)} && (39)\\ &+ (1-\theta)\Delta t[L(u^n) - A(u^n)]u^n + M_L q^{n+\theta}, && (40) \end{aligned}$$

where A is a nonlinear antidiffusion operator to be defined below. If it is omitted, we recover the low-order discretization of upwind type which is nonoscillatory but overdiffusive. The objective is to add as much antidiffusion as possible without generating wiggles.

Importantly, A should be required to possess the zero row/column sum property. This ensures that the difference $D - A$ between $K^* = L - A$ and the original transport operator K is a generalized diffusion operator. Hence, the diffusive-antidiffusive terms can be decomposed into skew-symmetric internodal fluxes

$$(K^*u)_i = \sum_j k_{ij}u_j + \sum_{j\neq i}(f_{ij}^d + f_{ij}^a), \tag{41}$$

where the diffusive flux $f_{ij}^d = d_{ij}(u_j - u_i)$ is opposed by the antidiffusive flux f_{ij}^a designed so as to comply with the LED principle for the discrete scheme. This can be accomplished by applying flux limiters of TVD type introduced in the next two sections. A closely related FEM-FCT formulation is presented in [15],[16],[19]. It is to be recommended for strongly time-dependent problems which call for the use of a consistent mass matrix.

6 Slope-limiter FEM-TVD scheme

For the solution to remain nonoscillatory, the antidiffusive flux f_{ij}^a from node j into node i must be interpretable as a diffusive flux from some other node(s). This prerequisite is satisfied by finite difference TVD schemes, cf. equation (13). A usable multidimensional extension can be derived by constructing the antidiffusive fluxes as follows

$$f_{ij}^a = \Phi(r_i)a_{ij}(u_i - u_j) = a_{ij}\mathcal{L}(u_i - u_j, \Delta u_{ij}), \qquad f_{ji}^a = -f_{ij}^a. \tag{42}$$

The net flux $f_{ij}^d + f_{ij}^a = (d_{ij} - \Phi(r_i)a_{ij})(u_j - u_i)$ depends on the antidiffusion coefficient a_{ij} and on the limiter Φ which is defined in terms of the limited average operator $\mathcal{L}$ as explained above. The 'upwind difference' Δu_{ij} is related to the 'slope ratio' r_i via the formula $\Delta u_{ij} = r_i(u_i - u_j)$. Let us leave a_{ij} and Δu_{ij} unspecified for the time being.

The antidiffusive fluxes are intended to reduce the error due to discrete upwinding. They are computed and plugged into the global defect vector $R(u)$ edge-by-edge. Each numerical edge $\vec{ij}$ is associated with two nonzero off-diagonal matrix entries. Recall that it links an upwind node i and a downwind node j according to the adopted convention. Given this orientation of the edge $\vec{ij}$, its share of the term K^*u can be written as

$$\text{node } i: \qquad k_{ij}^*(u_j - u_i) = \Phi(r_i)a_{ij}(u_i - u_j) = \Phi(1/r_i)a_{ij}\Delta u_{ij}, \tag{43}$$

$$\text{node } j: \qquad k_{ji}^*(u_i - u_j) = (l_{ji} - \Phi(r_i)a_{ij})(u_i - u_j). \tag{44}$$

The contribution to node j is of diffusive nature and leads to a LED discretization as long as the coefficient k_{ji}^* is nonnegative, i.e. $\Phi(r_i)a_{ij} \le l_{ji}$. This condition is always satisfied by one-dimensional TVD schemes with $a_{ij} = d_{ij}$. As shown in [15],[16], discrete upwinding for the pure convection equation discretized on a uniform mesh results in the standard upwind difference approximation with $l_{ji} = 2d_{ij} = v$. It follows that $k_{ji}^* = (2-\Phi(r_i))v \ge 0$, since all of the flux limiters presented above satisfy the inequality $0 \le \Phi(r) \le 2$.

A safe choice of the antidiffusion coefficient a_{ij} which ensures that the coefficient k_{ji}^* is nonnegative for an arbitrary value of the slope ratio r_i is given by $a_{ij} = \min\{d_{ij}, l_{ji}/2\}$. Alternatively, the concrete value of the correction factor $\Phi(r_i)$ can be taken into account to provide a better estimate of admissible antidiffusion

$$a_{ij} = \min\{d_{ij}, l_{ji}/\Phi(r_i)\}. \tag{45}$$

This is equivalent to using the antidiffusive flux $f_{ij}^a = \min\{\Phi(r_i)d_{ij}, l_{ji}\}(u_i - u_j)$.

In any case, the edge contribution to node i will also exhibit the desired LED structure provided that the upwind difference Δu_{ij} can be cast in the form

$$\Delta u_{ij} = \sum_{k \ne i} c_{ik}(u_k - u_i), \qquad \text{where} \quad c_{ik} \ge 0. \tag{46}$$

In one-dimensional TVD schemes, the quantity r_i represents the slope ratio (11) at the upwind node, so that $\Delta u_{ij} = u_k - u_i$, where $k \ne j$ refers to the second neighbor of node i. However, the choice of Δu_{ij} for finite element discretizations on unstructured meshes is nontrivial. A geometric approach commonly employed in the literature is to reconstruct

a local one-dimensional stencil by introducing two dummy nodes on the continuation of the edge $\vec{ij}$ [1],[11],[26],[27]. The difference Δu_{ij} is defined as in one dimension using the interpolated or extrapolated solution value at the dummy node k adjacent to the upwind node i. The reconstructed stencil for a triangular mesh is shown in Figure 2.

The numerical behavior of various techniques for the recovery of u_k was analyzed in detail by Lyra [26]. A comparative study was conducted for the following algorithms:

1. Interpolation/extrapolation using the adjacent triangle T_i containing node i.

2. Interpolation using the actual triangle T_k containing the dummy node k.

3. Extrapolation using a least squares reconstruction for the gradient at node i.

Numerical experiments revealed that solutions depend strongly on the employed strategy. The first option was proved to provide the LED property but failed to produce nonoscillatory results for some aerodynamic applications. The second procedure based on the actual triangle was favored due to the enhanced robustness as compared to the use of the adjacent triangle. However, the resulting discretization is no longer local extremum diminishing and neither is the gradient reconstruction method which corresponds to

$$\Delta u_{ij} = (\mathbf{x}_i - \mathbf{x}_j) \cdot \nabla_h u_i, \qquad \text{where} \qquad \nabla_h u_i = \frac{1}{m_i} \sum_{k \neq i} \mathbf{c}_{ki} (u_k - u_i). \tag{47}$$

Here $\nabla_h u_i$ stands for a continuous approximation to the solution gradient at the upwind node i recovered by means of a consistent L_2-projection. The involved coefficients $\mathbf{c}_{ki}$ are defined by (19) for the standard Galerkin method. This approach is very attractive from the standpoint of implementation and memory requirements. However, Lyra [26] reported its performance to be quite poor and emphasized the need for the development of a more robust algorithm for the reconstruction of nodal gradients.

Let us explain why the above choice of the upwind difference is unsatisfactory. If any of the factors $\mathbf{c}_{ki} \cdot (\mathbf{x}_i - \mathbf{x}_j)$ in the formula for Δu_{ij} is negative, then it does not admit the representation (46) which is necessary to satisfy the LED criterion. To rectify this, we can

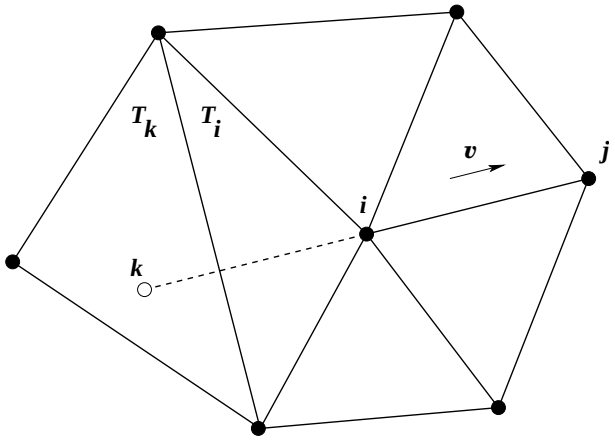

Figure 2. Three-point stencil in two dimensions.

employ a monotone projection operator constructed by resorting to discrete upwinding. Note that $\mathbf{c}_{ki} = -\mathbf{c}_{ik}$ (for internal nodes), so that the elimination of negative off-diagonal coefficients leads to the following LED-type reconstruction procedure

$$\Delta u_{ij} = \frac{2}{m_i} \sum_{k \neq i} \max\{0, \mathbf{c}_{ki} \cdot (\mathbf{x}_i - \mathbf{x}_j)\}(u_k - u_i). \tag{48}$$

For uniform meshes in one dimension, this kind of extrapolation corresponds to using the upwind gradient and yields the standard value $\Delta u_{ij} = u_k - u_i$.

The upwind difference Δu_{ij} can be readily converted into the slope ratio r_i which serves as the smoothness indicator for the TVD limiter. Hence, the proposed modification of the Galerkin method will be referred to as the slope-limiter FEM-TVD scheme. Unlike the edge-based algorithm of Lyra *et al.* [27], it is applicable to arbitrary finite elements and is guaranteed to satisfy the LED criterion. In our experience, it produces excellent simulation results for a wide range of CFD applications as complex as reactive bubbly flows in gas-liquid reactors [18]. At the same time, algorithms based on stencil reconstruction depend on geometric details of the underlying mesh and require a great deal of bookkeeping. Even the presented gradient recovery method needs the coordinates of the mesh nodes to construct the upwind difference.

Slope-limiter FEM-TVD schemes may also exhibit poor convergence rates for some steady-state problems such as the incompressible flow around a cylinder simulated using nonconforming FEM on an unstructured mesh (see below). This shortcoming was also mentioned by Lyra [26] who attributed it to the lack of background dissipation and indicated that convergence rates can be improved to some extent by 'freezing' the antidiffusive terms as the solution approaches the steady state. To keep things simple and avoid using questionable remedies, let us proceed to the derivation of an alternative formulation which appears to offer a truly multidimensional generalization of the TVD methodology.

7 Flux-limiter FEM-TVD scheme

Returning to the definition (11), we remark that the quantity r_i can be interpreted as the ratio of fluxes rather than slopes as long as the velocity v is constant. This observation leads to the new family of FEM-TVD schemes proposed in this section.

The original transport operator K violates the LED constraint, since its off-diagonal entries are of variable sign. Let us split the contribution of the incompressible part to node i into a sum with positive coefficients and a sum with negative coefficients

$$\sum_{j \neq i} k_{ij}(u_j - u_i) = P_i + Q_i, \tag{49}$$

which in turn consist of positive and negative flux components

$$P_i = P_i^+ + P_i^-, \qquad P_i^\pm = \sum_{j \neq i} \max\{0, k_{ij}\} \begin{matrix} \max \\ \min \end{matrix} \{0, u_j - u_i\}, \tag{50}$$

$$Q_i = Q_i^+ + Q_i^-, \qquad Q_i^\pm = \sum_{j \neq i} \min\{0, k_{ij}\} \begin{matrix} \min \\ \max \end{matrix} \{0, u_j - u_i\}. \tag{51}$$

In essence, P_i represents the total diffusive contribution and Q_i the total antidiffusive contribution to node i. According to the LED principle, diffusive fluxes are harmless. Nonphysical oscillations are caused by the antidiffusive ones which need to be controlled. Discrete upwinding eliminates negative off-diagonal coefficients completely while increasing positive ones. This brute-force approach substantially exaggerates the diffusive fluxes and is not to be recommended *per se* because of the pronounced smearing it incurs as a result. As already mentioned, (a certain portion of) an antidiffusive flux can be retained (or even enhanced) if it behaves as a diffusive flux for the concrete solution.

The Galerkin (central difference) method for the one-dimensional convection equation can be written in the form (5) with $c_{i-1/2} = -c_{i+1/2} = v/(2\Delta x)$. Hence, we infer that node i receives the diffusive contribution $P_i = c_{i-1/2}(u_{i-1} - u_i)$ from its upwind neighbor and the antidiffusive contribution $Q_i = c_{i+1/2}(u_{i+1} - u_i)$ from its downwind neighbor. The flux limiter examines the ratio $r_i = P_i/Q_i$ and makes sure that the net increment to node i is diffusive enough to suppress nonphysical undershoots and overshoots. Recall that $\Phi(r_i) = 0$ unless $r_i > 0$, which means that no antidiffusion is added if P_i and Q_i are of the opposite sign. In other words, $P_i^\pm$ and $Q_i^\pm$ must act in concert.

In the multidimensional case, the contribution Q_i is composed from the raw antidiffusive fluxes $-f_{ij}^d = d_{ij}(u_i - u_j)$ which must be multiplied by appropriate correction factors. The crux of our new algorithm is to apply a TVD limiter Φ to the ratio $P_i^\pm/Q_i^\pm$ depending on the sign of the flux. To this end, let us introduce the nodal correction factors

$$R_i^\pm = \Phi(P_i^\pm/Q_i^\pm) \tag{52}$$

responsible for the positive/negative antidiffusive fluxes associated with numerical edges for which i is the upwind node. It is possible to take $R_i^\pm = 1$ for nodes at which Dirichlet boundary conditions are prescribed, because in a typical implementation the off-diagonal entries of the corresponding matrix rows are overwritten by zeros anyway.

To ensure that the coefficient k_{ji}^* of the modified transport operator K^* is nonnegative, the antidiffusive flux f_{ij}^a is designed as follows

$$f_{ij}^a = \begin{cases} \min\{R_i^+ d_{ij}, l_{ji}\}(u_i - u_j), & \text{if } u_i > u_j, \\ \min\{R_i^- d_{ij}, l_{ji}\}(u_i - u_j), & \text{if } u_i < u_j, \\ 0, & \text{if } u_i = u_j. \end{cases} \tag{53}$$

The contribution of the edge $\vec{ij}$ to the global defect vector within the term K^*u can be represented by the formulae (43)–(45) provided that the ratio r_i is redefined as

$$r_i = \begin{cases} P_i^+/Q_i^+, & \text{if } u_i > u_j, \\ P_i^-/Q_i^-, & \text{if } u_i < u_j. \end{cases} \tag{54}$$

By construction, $\Delta u_{ij} = r_i(u_i - u_j)$ is of the form (46), which proves the LED property.

The above algorithm will be called the flux-limiter FEM-TVD method to distinguish it from the slope-limiter approach described in the preceding section. In one dimension, both generalizations reduce to their finite difference prototype. The node-oriented limiting strategy introduced in this section is akin to that proposed by Zalesak [39] but operates on entirely different premises. It seems to be much more robust than the unidirectional slope limiting which is strongly influenced by the alignment of the reconstructed stencil and by the method employed to recover the solution values at dummy nodes.

8 Summary of the algorithm

The proposed multidimensional generalization of TVD schemes can be implemented on arbitrary grids using either the conventional or the edge-based data structure. As a matter of fact, the algorithm is applicable to finite differences, finite elements and finite volumes alike, since it operates with discrete transport operators regardless of their origin. The required modifications are limited to the matrix assembly routine provided that the code is already equipped with a defect correction loop of type (35) for an iterative treatment of nonlinearities. The postprocessing steps to be performed can be summarized as follows:

In a loop over edges:

1. Retrieve the entries k_{ij} and k_{ji} of the high-order transport operator.
2. Determine the artificial diffusion coefficient d_{ij} from equation (33).
3. Update the four entries of the preconditioner C as required by (34).
4. Adopt the 'upwind-downwind' edge orientation $\vec{ij}$ such that $l_{ij} \leq l_{ji}$.
5. Store the coefficients d_{ij} and $l_{ji} = |k_{ji} - k_{ij}|$ for future reference.

In a loop over nodes:

6. Calculate the diffusive/antidiffusive contributions $P_i^{\pm}$ and $Q_i^{\pm}$.
7. Apply a TVD limiter Φ to obtain the nodal correction factors $R_i^{\pm}$.

In a loop over edges:

8. Compute the diffusive flux $f_{ij}^d = d_{ij}(u_j - u_i)$ due to discrete upwinding.
9. Evaluate the nonlinear antidiffusive flux f_{ij}^a from the formula (53).
10. Insert the net diffusive flux $f_{ij} = f_{ij}^d + f_{ij}^a$ into the defect vector R.

The slope-limiter FEM-TVD method can be coded in a similar fashion using the upwind difference (48) to determine the slope ratio $r_i = \Delta u_{ij}/(u_i - u_j)$ and the corresponding correction factors $\Phi(r_i)$. Note that no loop over nodes is needed in this case. Indeed, the recovery of Δu_{ij} via stencil reconstruction is performed independently for each edge. As an alarming consequence, the contributions of other edges are not taken into account, so that the total antidiffusive flux $\sum_{j \neq i} f_{ij}^a$ cannot be properly controlled.

9 Numerical examples

In the examples which follow, we study the performance of the flux-limiter FEM-TVD algorithm. In our experience, the slope-limiter version yields essentially the same results on Cartesian grids but is rather cumbersome, expensive and less robust than the multidimensional flux limiter introduced in this paper. As far as the time discretization is concerned, we restrict ourselves to implicit schemes which are unconditionally stable and much more efficient than explicit ones unless the time step must remain small for accuracy reasons. Semi-implicit FEM-TVD schemes ($0 < \theta < 1$) are positivity-preserving under a CFL-like condition which can be derived as explained in [15],[16].

9.1 Solid body rotation

Rotation of solid bodies with discontinuities and small scale features is frequently used as a challenging test problem for transport algorithms. In the first example, we consider the benchmark configuration proposed by LeVeque [22]. It is intended to examine the ability of a numerical method to reproduce both discontinuous and smooth profiles. To this end, a slotted cylinder, a cone and a smooth hump are exposed to the nonuniform velocity field $\mathbf{v} = (0.5 - y, x - 0.5)$ and undergo a counterclockwise rotation about the center of the square domain $\Omega = (0,1) \times (0,1)$. Each of these bodies lies within a circle of radius $r_0 = 0.15$ centered at a point with Cartesian coordinates (x_0, y_0).

The exact solution to the pure convection equation after each full revolution matches the initial data depicted in Figure 3 (left). Let us introduce the normalized distance function $r(x,y) = \frac{1}{r_0}\sqrt{(x-x_0)^2 + (y-y_0)^2}$. It follows that $u(x,y,0) = 0$ for $r(x,y) > 1$. Elsewhere, the reference shape of the three bodies is given by

$$\begin{aligned}
&\text{Cylinder:} && (x_0, y_0) = (0.5, 0.75), && u(x,y,0) = \begin{cases} 1, & \text{if } |x - x_0| \geq 0.025 \vee y \geq 0.85, \\ 0, & \text{otherwise.} \end{cases} \\
&\text{Cone:} && (x_0, y_0) = (0.5, 0.25), && u(x,y,0) = 1 - r(x,y). \\
&\text{Hump:} && (x_0, y_0) = (0.25, 0.5), && u(x,y,0) = 0.25[1 + \cos(\pi \min\{r(x,y), 1\})].
\end{aligned}$$

The numerical solution at $t = 2\pi$ produced by the FEM-TVD scheme with the Crank-Nicolson time-stepping and the superbee flux limiter is shown in Figure 3 (right). It was computed on a uniform mesh of 128×128 bilinear elements using the time step $\Delta t = 10^{-3}$.

No spurious wiggles are observed and the resolution of discontinuities is far superior to that achievable with discrete upwind or a similar low-order method. Even the narrow bridge of the slotted cylinder is largely preserved. However, the irrecoverable error induced by mass lumping leads to some loss of accuracy which manifests itself in a noticeable erosion of the ridges. Furthermore, the employed superbee limiter is known to be slightly underdiffusive (see the next example), which results in an artificial steepening of solution gradients and a pronounced peak flattening for the cone and hump.

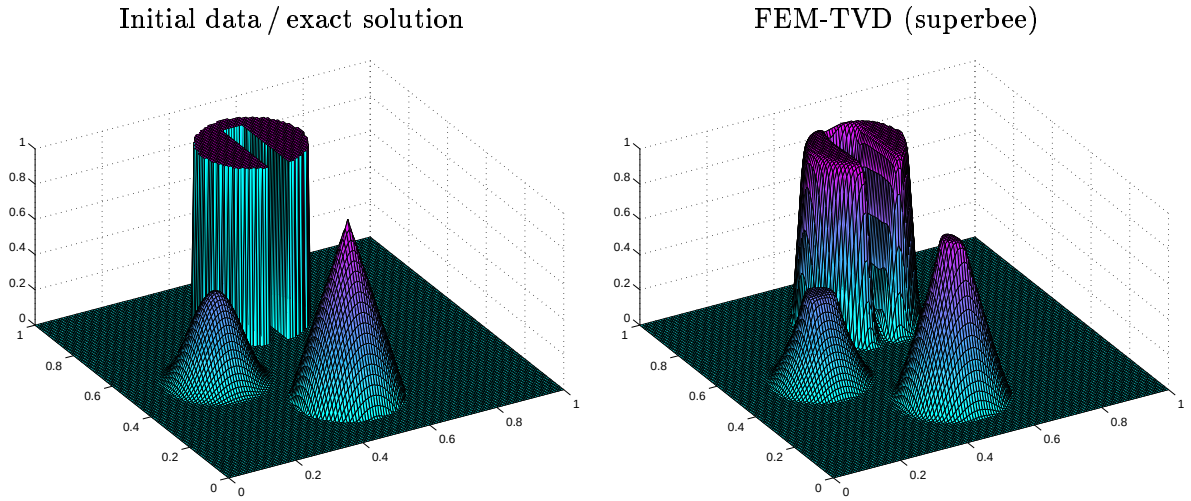

Figure 3. Solid body rotation, 128×128 bilinear elements, $t = 2\pi$.

9.2 Rotation of a Gaussian hill

The second test case proposed by Lapin [20] makes it possible to evaluate the magnitude of artificial diffusion due to the discretization in space and time. This can be accomplished by applying certain statistical tools to the convection-diffusion equation

$$\frac{\partial u}{\partial t} + \mathbf{v} \cdot \nabla u = \epsilon \Delta u \quad \text{in } \Omega = (-1,1) \times (-1,1), \tag{55}$$

where $\mathbf{v} = (-y, x)$ is the velocity field and $\epsilon = 10^{-3}$ is the physical diffusion coefficient.

The initial condition to be imposed is given by $u(x, y, 0) = \delta(x_0, y_0)$, where δ stands for the Dirac delta function. Clearly, it is impossible to initialize the solution by a singular function in a practical implementation. Instead, it is reasonable to concentrate the whole mass at a single node. The integral of a discrete function over the domain Ω can be computed as the sum of nodal values multiplied by the entries of the lumped mass matrix: $\int_\Omega u_h \, d\mathbf{x} = \int_\Omega \sum_i u_i \varphi_i \, d\mathbf{x} = \sum_i m_i u_i$. The total mass of a delta function equals unity. Hence, one should find node i closest to the peak location (x_0, y_0) and set $u_i^0 = 1/m_i$, $u_j^0 = 0, \ j \neq i$. Alternatively, one can start with the exact solution at a time $t_0 > 0$.

In the rotating Lagrangian reference frame, the convective term vanishes and the resulting diffusion problem can be solved analytically. It can be readily verified that the exact solution of (55) is a Gaussian hill defined by the normal distribution function

$$u(x, y, t) = \frac{1}{4\pi\epsilon t} \, e^{-\frac{r^2}{4\epsilon t}}, \qquad r^2 = (x - \hat{x})^2 + (y - \hat{y})^2,$$

where $\hat{x}$ and $\hat{y}$ denote the time-dependent peak coordinates

$$\hat{x}(t) = x_0 \cos t - y_0 \sin t, \qquad \hat{y}(t) = -x_0 \sin t + y_0 \cos t.$$

The actual peak coordinates for a numerical approximation may be quite different. They can be calculated as the mathematical expectation of the center of mass under the probability distribution with density u_h given by the finite element solution

$$\hat{x}_h(t) = \int_\Omega x u_h(x, y, t) \, d\mathbf{x}, \qquad \hat{y}_h(t) = \int_\Omega y u_h(x, y, t) \, d\mathbf{x}.$$

The quality of approximation can be assessed by considering the standard deviation

$$\sigma_h^2(t) = \int_\Omega r_h^2 u_h(x, y, t) \, d\mathbf{x}, \qquad r_h^2 = (x - \hat{x}_h)^2 + (y - \hat{y}_h)^2,$$

which quantifies the rate of smearing caused by both physical and the numerical diffusion. Due to all sorts of discretization errors, σ_h^2 may differ considerably from the exact value $\sigma^2 = 4\epsilon t$. This discrepancy represented by the relative variance error

$$\Delta\sigma_{\text{rel}} = \frac{\sigma_h^2 - \sigma^2}{\sigma^2} = \frac{\sigma_h^2}{4\epsilon t} - 1$$

serves as an excellent indicator of numerical diffusion inherent to the discretization scheme.

Exact solution, $||u||_\infty = 10.1360$ FEM-TVD (MC), $||u||_\infty = 9.9283$

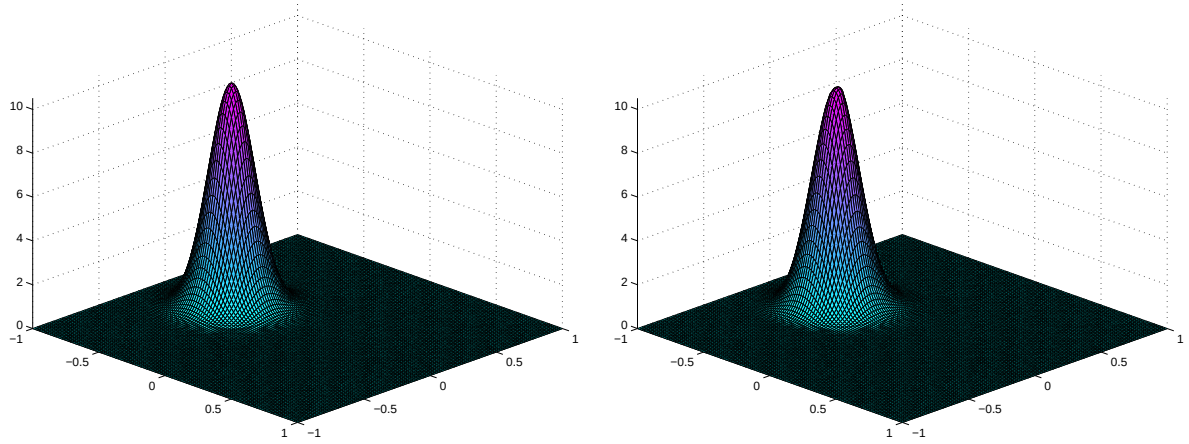

Figure 4. Rotation of a Gaussian hill, 128×128 bilinear elements, $t = 2.5\,\pi$.

Let us start with the analytical solution corresponding to $x_0 = 0$, $y_0 = 0.5$ and $t_0 = 0.5\,\pi$. Figure 4 depicts the exact and numerical solution after one full revolution of the Gaussian hill. The mesh size and time step are the same as in the previous example. The solution produced by the FEM-TVD method with the Crank-Nicolson time-stepping and the MC flux limiter proves to be very accurate, although some 'peak clipping' does occur. The global maximum drops to 9.9283 as compared to 10.1360 for the exact solution.

As the Gaussian hill moves around the origin, it is being gradually smeared by diffusion. The error estimator $\Delta\sigma_{\text{rel}}$ enables us to compare the performance of standard TVD limiters and to investigate the influence of the time discretization. If the first-order accurate backward Euler method is employed, the temporal part of the relative variance error plays an important role at large time steps and decreases linearly as the time step is refined (see Figure 5, left). For the second-order accurate Crank-Nicolson scheme, the temporal discretization error is negligibly small. This is why the time step does not affect the values of $\Delta\sigma_{\text{rel}}$ displayed in Figure 5 (right). In this case, the accuracy is determined by the space discretization and the choice of the flux limiter is decisive.

Backward Euler scheme Crank-Nicolson scheme

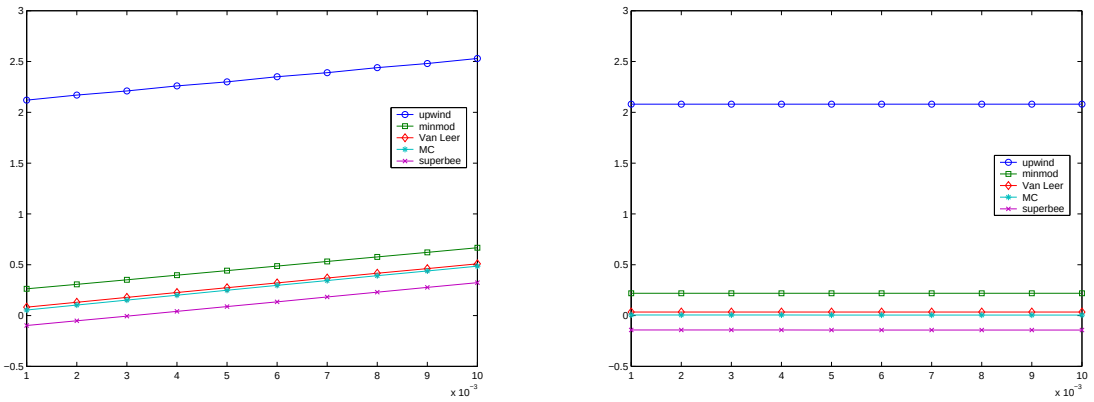

Figure 5. Gaussian hill: relative variance error vs. the time step.

As expected, by far the most diffusive solutions are produced by the discrete upwind scheme, whereas the nonlinear FEM-TVD correction leads to a dramatic improvement. At the same time, a comparison of standard TVD limiters with one another reveals that the relative variance error may differ appreciably from case to case. The most diffusive limiter is minmod followed by Van Leer. The MC limiter used to obtain the numerical solution shown in Figure 4 outperforms both of them. Moreover, it is more suitable for the treatment of smooth profiles than Roe's superbee limiter. The latter turns out to be underdiffusive, so that $\Delta\sigma_{\text{rel}}$ is negative if the spatial discretization error dominates. It is important to be aware of this fact when using the superbee limiter in CFD simulations.

9.3 Steady-state convection-diffusion

The FEM-TVD algorithm for the design of discrete transport operators can be applied to stationary problems directly or in conjunction with a pseudo-time-stepping technique. In the latter case, the steady-state solution is obtained by marching into the stationary limit of the associated time-dependent problem. The temporal accuracy is immaterial in this case, since the time step is merely an artificial parameter which determines the convergence rates. Hence, it is desirable to choose time steps as large as possible, so as to reduce the computational cost. The restrictive CFL condition prevents explicit schemes from operating with large time steps and makes them too inefficient for our purposes. This drawback can be rectified to some extent by resorting to local time-stepping but it is obvious that steady-state problems call for an implicit treatment.

In light of the above, the fully implicit backward Euler method, which was found to be quite diffusive for transient problems, constitutes an excellent iterative solver for steady or creeping flows. Let us investigate the numerical behavior of the BE/TVD scheme for the singularly perturbed convection-diffusion equation

$$\mathbf{v} \cdot \nabla u - \epsilon \Delta u = 0 \qquad \text{in } \Omega = (0,1) \times (0,1),$$

where $\mathbf{v} = (\cos 10^{\text{o}}, \sin 10^{\text{o}})$ and $\epsilon = 10^{-3}$. The concomitant boundary conditions read

$$\frac{\partial u}{\partial y}(x,1) = 0, \qquad u(x,0) = u(1,y) = 0, \qquad u(0,y) = \begin{cases} 1, & y \geq 0.5, \\ 0, & y < 0.5. \end{cases}$$

The solution to this elliptic problem is characterized by the presence of a sharp front next to the line $x = 1$. The boundary layer develops because the solution of the reduced problem ($\epsilon = 0$) does not satisfy the homogeneous Dirichlet boundary condition.

A reasonable initial approximation for the pseudo-time-stepping loop is given by

$$u(x,y,0) = \begin{cases} 1 - x, & y \geq 0.5, \\ 0, & y < 0.5. \end{cases}$$

It is worthwhile to start with the discrete upwind scheme and use the converged low-order solution as initial data for the time-dependent FEM-TVD algorithm. This 'educated guess' should be close enough to the steady-state limit. Hence, the computational overhead due to the assembly and limiting of antidiffusive fluxes will be insignificant.

The numerical solutions depicted in Figure 6 demonstrate that the FEM-TVD method combined with backward Euler time discretization is capable of producing nonoscillatory solutions with a sharp resolution of steep fronts and boundary layers. The upper two diagrams were computed as before on the Cartesian grid of 128×128 bilinear elements, while the computational mesh for the lower ones is much coarser, as is clearly seen from the 2D plots shown on the right. The nonuniform mesh consists of 1920 elements and is refined in regions where the solution gradients are large. Due to the adaptive mesh refinement and a special alignment of the grid lines, the accuracy is comparable with that achieved on the uniform mesh at a much higher computational cost. This example indicates that our multidimensional FEM-TVD algorithm can be successfully applied on adaptive meshes and benefit from the unconditional stability of implicit time-stepping, which is not the case for most other high resolution schemes available to date.

Uniform mesh, 128×128 bilinear elements.

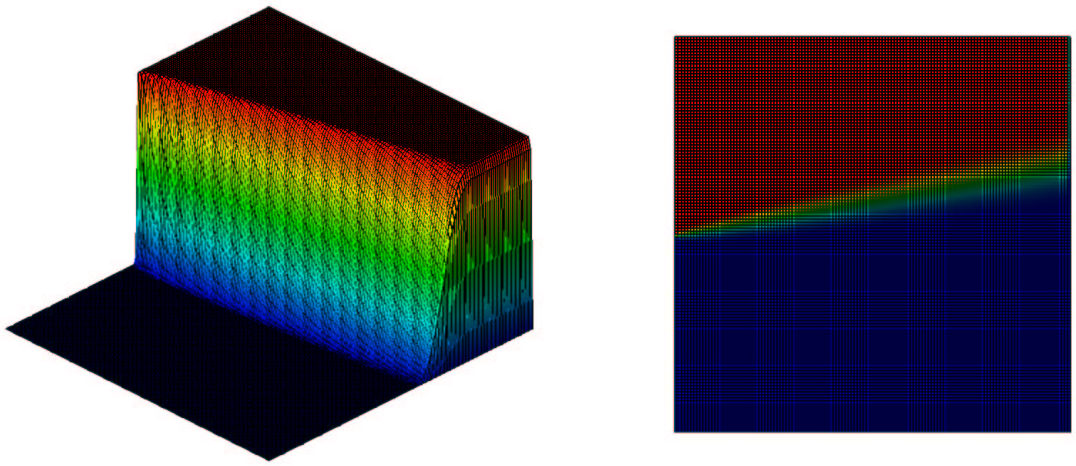

Nonuniform mesh, 1920 bilinear elements.

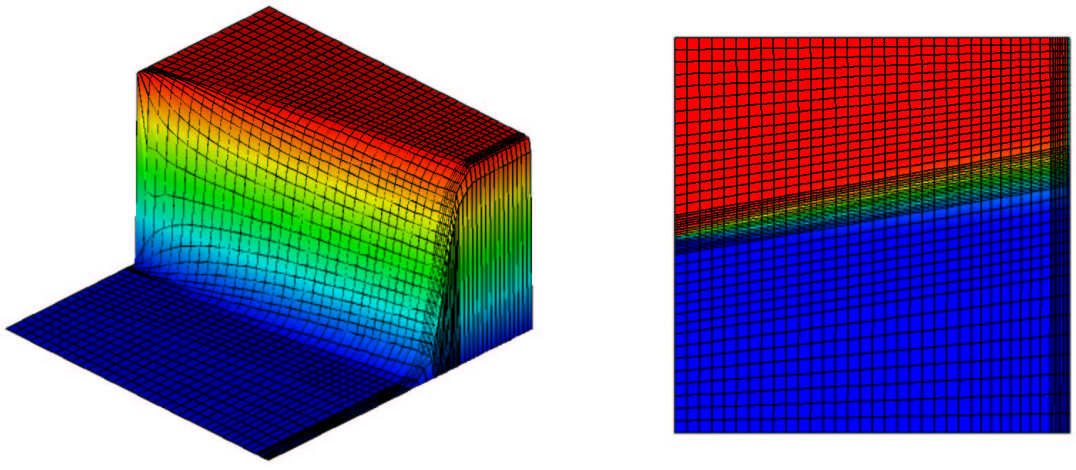

Figure 6. Convection-diffusion, $\epsilon = 10^{-3}$. FEM-TVD (superbee).

9.4 Standing vortex

The generality of the fully discrete approach has enabled us to integrate the FEM-TVD algorithm into the incompressible flow solver FEATFLOW based on the nonconforming Rannacher-Turek finite elements [31],[37]. The multidimensional flux limiter was built into the matrix assembly routine for the nonlinear convective terms and proved its worth for the (discontinuous) rotated bi-/trilinear approximation of velocity components on irregular quadrilateral/hexahedral meshes. The incompressibility constraint for the Navier-Stokes equations was imposed in the framework of the Multilevel Pressure Schur Complement formulation which unites coupled solution techniques and discrete projection methods which decouple the velocity and pressure using suitable operator-splitting tools [38].

Let us first apply a nonstationary projection solver to the well-known *standing vortex* problem in order to verify the dissipative properties of TVD limiters. The incompressible Navier-Stokes equations for an inviscid flow ($Re = \infty$) are solved in a unit square

$$\begin{aligned} &\frac{\partial \mathbf{u}}{\partial t} + \mathbf{u} \cdot \nabla \mathbf{u} + \nabla p = 0 \\ &\nabla \cdot \mathbf{u} = 0 \end{aligned} \qquad \text{in } \Omega = (0,1) \times (0,1).$$

The initial condition is an axisymmetric vortex which also represents the exact steady-state solution. In polar coordinates, the velocity $\mathbf{u}$ can be decomposed into the radial component u_r and the angular component u_θ which are initialized by

$$u_r = 0, \qquad u_\theta = \begin{cases} 5r, & r < 0.2, \\ 2 - 5r, & 0.2 \le r \le 0.4, \\ 0, & r > 0.4, \end{cases}$$

where $r = \sqrt{(x-0.5)^2 + (y-0.5)^2}$ denotes the distance from the center.

The objective is to test the ability of the discretization scheme to reproduce the original vortex. The numerical results produced by the Galerkin method equipped with discrete upwinding and four standard TVD limiters are compared to the exact solution in Figure 7. They were obtained at $t = 3$ using a mesh of 64×64 quadrilateral elements and backward Euler time-stepping. The artificial viscosity introduced by discrete upwinding is seen to have a devastating effect on the accuracy of the solution, while FEM-TVD injects enough antidiffusion to alleviate the smearing of the vortex. The differences between the performance of the flux limiters under consideration are marginal but a closer look reveals that their diffusivities compare as discussed above for the Gaussian hill problem.

9.5 Flow around a cylinder

The second incompressible flow problem to be dealt with is the established benchmark *Flow around a cylinder* developed for the priority program "Flow simulation on high-performance computers" under the auspices of DFG, the German Research Association [32]. This project was intended to facilitate the evaluation of various numerical algorithms for the incompressible Navier-Stokes equations in the laminar flow regime. A quantitative comparison of simulation results is possible on the basis of relevant flow characteristics such as drag and lift coefficients, for which reliable reference values are available. Moreover, the efficiency of solution techniques can be assessed in an objective manner.

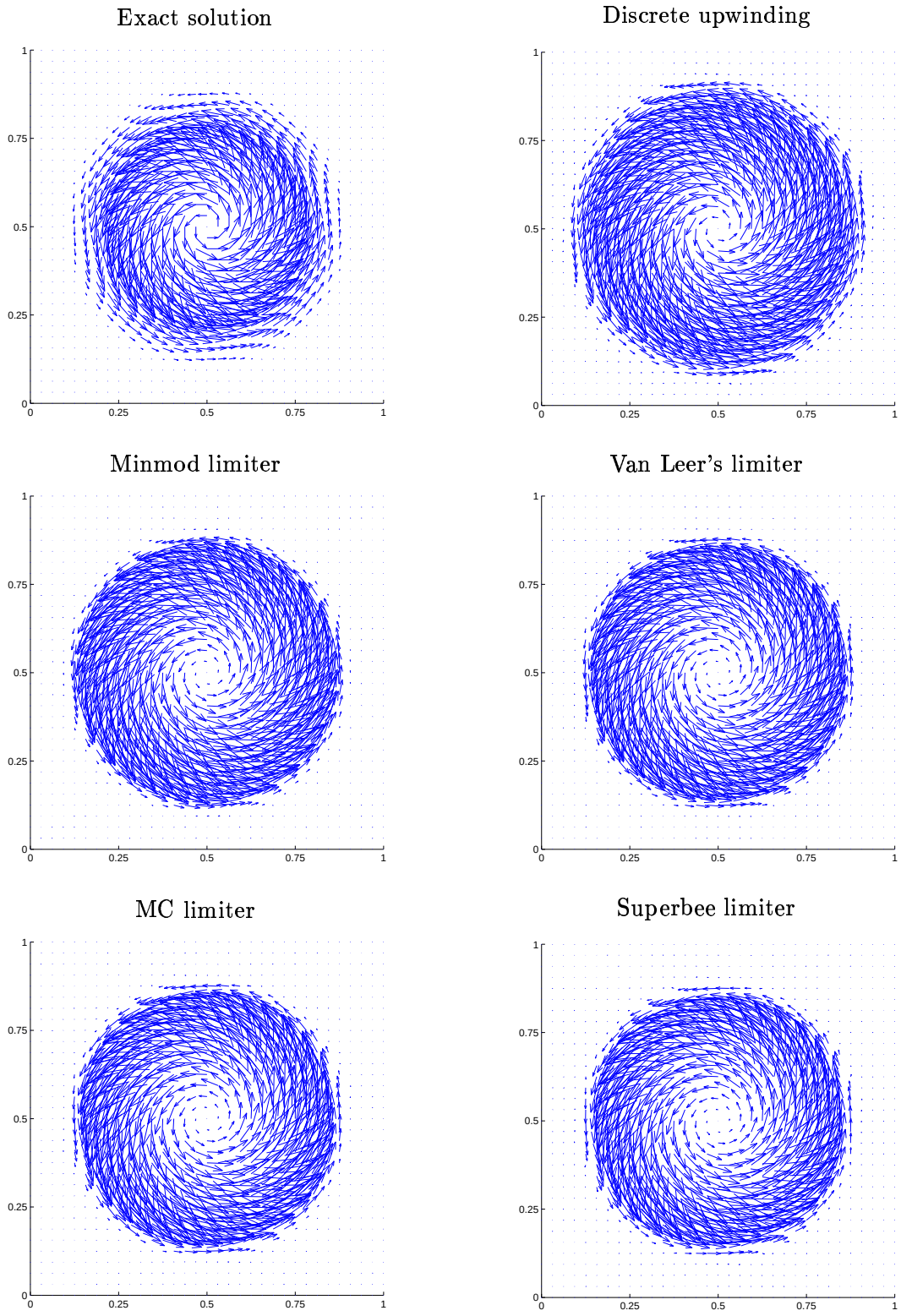

Figure 7. Standing vortex problem. FEM-TVD solution at $t = 3$.

Let us consider the steady incompressible flow around a cylinder with a circular cross-section. An in-depth description of the geometrical details and boundary conditions for the 2D/3D case can be found in references [32],[38] which contain all relevant information regarding this benchmark configuration. The flow at $Re = 20$ is actually dominated by diffusion and could be simulated by the standard Galerkin method without any extra stabilization (as far as the discretization is concerned; the iterative solver may require using a stabilized preconditioner). Our goal is to investigate the behavior of FEM-TVD schemes for such low Reynolds number flows, which fall outside the scope of their jurisdiction.

In particular, it is instructive to study the interplay of finite element discretizations for the convective and diffusive terms. As already mentioned above, discrete upwinding can be performed for the cumulative transport operator or just for the convective part. In the case of the nonconforming $\tilde{Q}_1$-elements, the discrete Laplacian operator originating from the Galerkin approximation of viscous terms is a positive-definite matrix but some of its off-diagonal coefficients are negative. Our numerical experiments indicate that it is worthwhile to leave it unchanged and apply the TVD postprocessing to the discretized convective term. In the case of linear or bilinear elements, physical diffusion can be taken into account in the formula (33) but the auxiliary quantities $P_i^{\pm}$ and $Q_i^{\pm}$ for the flux limiter should still be evaluated using the coefficients of the convective operator.

To generate the hierarchical data structures for the geometric multigrid algorithm which constitutes the core of our incompressible flow solver FEATFLOW, we introduce a sequence of successively refined quadrilateral meshes. The elements of the coarse mesh shown in Figure 8 are subdivided into four subelements at each refinement level, and the 2D mesh is extended into the third dimension for a 3D simulation. The two-dimensional results produced by the FEM-TVD algorithm embedded in a discrete projection method with pseudo-time-stepping are presented in Table 1. The computational mesh for the multigrid level NLEV contains NMT midpoints and NEL elements. For the employed $\tilde{Q}_1/Q_0$ finite element pair (rotated bilinear velocity, piecewise constant pressure), NMT represents the number of unknowns for each velocity component, while NEL equals the number of degrees of freedom associated with the pressure.

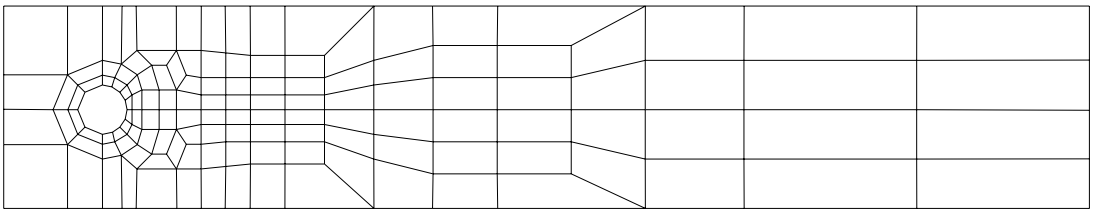

Figure 8. Coarse mesh for the DFG benchmark "Flow around a cylinder".

The drag and lift coefficients listed in Table 1 exhibit a monotone convergence behavior but fall short of the reference values $C_D \approx 5.5795$, $C_L \approx 0.01061$ on fine meshes. This discrepancy can be attributed to the inexact evaluation of surface integrals. Furthermore, the accuracy of approximation for such derived quantities cannot be properly controlled in a flow solver developed primarily for genuinely time-dependent problems. Fortunately, the FEM-TVD algorithm is readily applicable in the stationary case, so that the use of pseudo-time-stepping is not mandatory. Taking advantage of this fact, we integrated TVD limiters

into another FEATFLOW module which lends itself to the solution of the stationary Navier-Stokes equations. It is based on the local Multilevel Pressure Schur Complement approach with adaptive patching, whereby small subproblems are solved exactly within an outer block-Gauss-Seidel/Jacobi iteration [33],[38]. This strongly coupled solution technique is very robust and far superior to projection schemes at low Reynolds numbers.

NLEV	NMT	NEL	C_D	C_L
3	4264	2080	5.6502	$0.5233 \cdot 10^{-2}$
4	16848	8320	5.5852	$0.8080 \cdot 10^{-2}$
5	66976	33280	5.5760	$0.9946 \cdot 10^{-2}$
6	267072	133120	5.5707	$0.1042 \cdot 10^{-1}$
7	1066624	532480	5.5692	$0.0963 \cdot 10^{-1}$

Table 1. FEM-TVD (MC), projection solver.

Tables 2 and 3 demonstrate that the drag and lift coefficients produced by the coupled solver are in a good agreement with the reference values and with those obtained using Samarski's upwind method based on a classical artificial viscosity which depends on the local Reynolds number [38]. It is worth mentioning that this finite-volume-like discretization of convective terms, which has traditionally been used in FEATFLOW, involves a free parameter which must be determined by trial and error. Clearly, the 'optimal' value is hard to find from *a priori* considerations. In addition, Samarski's hybrid method is only suitable for intermediate and low Reynolds numbers, since it becomes increasingly diffusive and degenerates into the standard upwind scheme in the limit of inviscid flow. At the same time, the nonlinear FEM-TVD discretization remains remarkably accurate for arbitrarily large Reynolds numbers (see the previous example), whereby the tradeoff between accuracy and stability is managed automatically by the flux limiter.

NLEV	C_D	C_L	NL	MG	CPU
3	5.8084	$0.1733 \cdot 10^{-2}$	22	33	38
4	5.6514	$0.7171 \cdot 10^{-2}$	10	19	87
5	5.6003	$0.9734 \cdot 10^{-2}$	8	15	291
6	5.5854	$0.1040 \cdot 10^{-1}$	7	13	1074
7	5.5811	$0.1058 \cdot 10^{-1}$	5	9	3144

Table 2. FEM-TVD (MC), coupled solver.

NLEV	C_D	C_L	NL	MG	CPU
3	5.6699	$0.5694 \cdot 10^{-2}$	9	26	29
4	5.6004	$0.9700 \cdot 10^{-2}$	8	22	98
5	5.5841	$0.1048 \cdot 10^{-1}$	7	19	364
6	5.5806	$0.1060 \cdot 10^{-1}$	6	16	1280
7	5.5798	$0.1061 \cdot 10^{-1}$	5	13	4390

Table 3. Samarski's upwind, coupled solver.

Note that the number of nonlinear iterations NL and linear multigrid steps MG reduces as the mesh is refined. Moreover, the improvement of convergence rates is faster than that for the hybrid upwind method which is more efficient than FEM-TVD on coarse meshes but less efficient on fine ones, as can be seen from the presented CPU times. In our experience, the differences are even more pronounced if Newton's method is employed. On the other hand, its advantages in comparison with the straightforward defect correction seem to fade at high Reynolds numbers, since the nonlinearity inherent to the discretization procedure plays an increasingly important role. In a nutshell, the design of robust and efficient iterative solvers for nonlinear high-resolution schemes with flux limiters is a nontrivial task, so there is a lot of room for further research.

Last but not least, it is worth mentioning that our 'black-box' postprocessing routine for the convective operator proved to be applicable in 3D without any modifications. The three-dimensional simulation results produced by the FEM-TVD algorithm combined with a projection solver from the FEATFLOW package are presented in Figure 9. The underlying mesh consists of 49152 hexahedral elements and gives rise to 151808 unknowns for each velocity component. Even though this mesh is rather coarse, the resulting drag coefficient $C_D = 6.0841$ falls into the range of reference values published in [32].

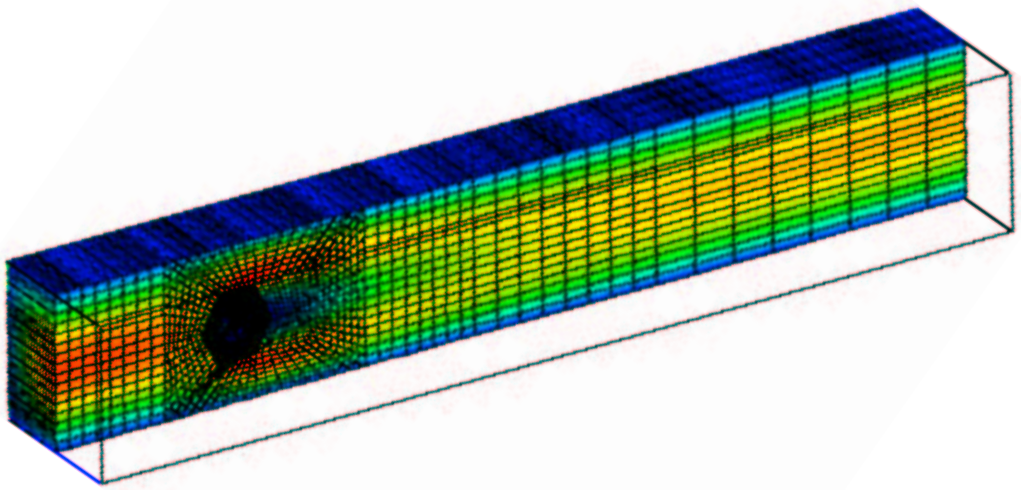

Figure 9. Horizontal velocity. FEM-TVD (MC), 3D projection solver.

10 Conclusions

A generalization of one-dimensional TVD schemes to finite element discretizations on unstructured meshes was presented. The discrete transport operator was modified by elimination of negative off-diagonal coefficients followed by insertion of compensating antidiffusion. The LED principle was utilized to generalize the concept of upwinding and to design a family of multidimensional TVD limiters controlling the local solution gradients or the ratio of diffusive/antidiffusive fluxes. The proposed algorithm renders an arbitrary discretization of convective terms local extremum diminishing and positivity-preserving.

It is characterized by a remarkable flexibility and the ease of implementation. Furthermore, it can be readily integrated into existing CFD software as a modular extension to the matrix assembly routine. The potential of the new methodology was demonstrated by application to scalar convection and incompressible flow problems. It can be extended to hyperbolic systems of conservation laws in the framework of an approximate Riemann solver using a suitable transformation to the characteristic variables (see [1],[3],[34],[35]).

Acknowledgments

The authors would like to thank Rainer Schmachtel for the implementation of FEM-TVD in the coupled Navier-Stokes solver and providing the data presented in Tables 2–3.

References

[1] P. Arminjon and A. Dervieux, Construction of TVD-like artificial viscosities on 2-dimensional arbitrary FEM grids. *INRIA Research Report* **1111** (1989).

[2] J. P. Boris and D. L. Book, Flux-corrected transport. I. SHASTA, A fluid transport algorithm that works. *J. Comput. Phys.* **11** (1973) 38–69.

[3] J. Donea, V. Selmin and L. Quartapelle, Recent developments of the Taylor-Galerkin method for the numerical solution of hyperbolic problems. *Numerical methods for fluid dynamics III*, Oxford, 171-185 (1988).

[4] J. H. Ferziger and M. Peric, *Computational Methods for Fluid Dynamics*. Springer, 1996.

[5] C. A. J. Fletcher, The group finite element formulation. *Comput. Methods Appl. Mech. Engrg.* **37** (1983) 225-243.

[6] S. K. Godunov, Finite difference method for numerical computation of discontinuous solutions of the equations of fluid dynamics. *Mat. Sbornik* **47** (1959) 271-306.

[7] P. Hansbo, Aspects of conservation in finite element flow computations. *Comput. Methods Appl. Mech. Engrg.* **117** (1994) 423-437.

[8] A. Harten, High resolution schemes for hyperbolic conservation laws, *J. Comput. Phys.* **49** (1983) 357–393.

[9] A. Harten, On a class of high resolution total-variation-stable finite-difference-schemes. *SIAM J. Numer. Anal* 21 (1984) 1-23.

[10] C. Hirsch, *Numerical Computation of Internal and External Flows. Vol. II: Computational Methods for Inviscid and Viscous Flows*. John Wiley & Sons, Chichester, 1990.

[11] A. Jameson, Analysis and design of numerical schemes for gas dynamics 1. Artificial diffusion, upwind biasing, limiters and their effect on accuracy and multigrid convergence, *International Journal of Computational Fluid Dynamics* **4** (1995) 171-218.

[12] A. Jameson, Computational algorithms for aerodynamic analysis and design. *Appl. Numer. Math.* **13** (1993) 383-422.

[13] A. Jameson, Positive schemes and shock modelling for compressible flows. *Int. J. Numer. Meth. Fluids* **20** (1995) 743–776.

[14] D. Kuzmin, Positive finite element schemes based on the flux-corrected transport procedure, In: *Computational Fluid and Solid Mechanics*, Elsevier, 887-888 (2001).

[15] D. Kuzmin and S. Turek, Flux correction tools for finite elements. *J. Comput. Phys.* **175** (2002) 525-558.

[16] D. Kuzmin, M. Möller and S. Turek, Multidimensional FEM-FCT schemes for arbitrary time-stepping. Technical report No. 215, University of Dortmund, 2002. To appear in *Int. J. Numer. Meth. Fluids.*

[17] D. Kuzmin, M. Möller and S. Turek, Implicit flux-corrected transport algorithm for finite element simulation of the compressible Euler equations. Technical report No. 221, University of Dortmund, 2002. To appear in: Proceedings of the Conference *Finite Element Methods: 50 Years of Conjugate Gradients*, University of Jyväskylä, Finland, June 11-12, 2002.

[18] D. Kuzmin and S. Turek, Finite element discretization and iterative solution techniques for multiphase flows in gas-liquid reactors. Technical report No. 222, University of Dortmund, 2002. To appear in: Proceedings of the Conference *Finite Element Methods: 50 Years of Conjugate Gradients*, University of Jyväskylä, Finland, June 11-12, 2002.

[19] D. Kuzmin, M. Möller and S. Turek, High-resolution FEM-FCT schemes for multidimensional conservation laws. Submitted to *Comput. Methods Appl. Mech. Engrg.*

[20] A. Lapin, University of Stuttgart. Private communication.

[21] R. J. LeVeque, *Numerical Methods for Conservation Laws*. Birkhäuser, 1992.

[22] R. J. LeVeque, High-resolution conservative algorithms for advection in incompressible flow. *Siam J. Numer. Anal.* **33** (1996) 627–665.

[23] R. Löhner, *Adaptive CFD Techniques*. Wiley, 2001.

[24] R. Löhner, K. Morgan, J. Peraire and M. Vahdati, Finite element flux-corrected transport (FEM-FCT) for the Euler and Navier-Stokes equations. *Int. J. Numer. Meth. Fluids* **7** (1987) 1093–1109.

[25] R. Löhner, K. Morgan, M. Vahdati, J. P. Boris and D. L. Book, FEM-FCT: combining unstructured grids with high resolution. *Commun. Appl. Numer. Methods* **4** (1988) 717–729.

[26] P. R. M. Lyra, *Unstructured Grid Adaptive Algorithms for Fluid Dynamics and Heat Conduction*. PhD thesis, University of Wales, Swansea, 1994.

[27] P. R. M. Lyra, K. Morgan, J. Peraire and J. Peiro, TVD algorithms for the solution of the compressible Euler equations on unstructured meshes. *Int. J. Numer. Meth. Fluids* **19** (1994) 827–847.

[28] K. Morgan and J. Peraire, Unstructured grid finite element methods for fluid mechanics. *Reports on Progress in Physics*, **61** (1998), no. 6, 569-638.

[29] S. V. Patankar, *Numerical Heat Transfer and Fluid Flow.* McGraw-Hill, New York, 1980.

[30] J. Peraire, M. Vahdati, J. Peiro and K. Morgan, The construction and behaviour of some unstructured grid algorithms for compressible flows. *Numerical Methods for Fluid Dynamics* **IV**, Oxford University Press, 221-239 (1993).

[31] R. Rannacher and S. Turek, A simple nonconforming quadrilateral Stokes element. *Numer. Meth. PDEs* **8** (1992), no. 2, 97-111.

[32] M. Schäfer and S. Turek (with support of F. Durst, E. Krause, R. Rannacher), Benchmark computations of laminar flow around cylinder, In E.H. Hirschel (ed.), *Flow Simulation with High-Performance Computers II*, Vol. 52 von *Notes on Numerical Fluid Mechanics*, Vieweg, 1996, 547–566.

[33] R. Schmachtel, *Robuste lineare und nichtlineare Lösungsverfahren für die inkompressiblen Navier-Stokes-Gleichungen.* PhD thesis, University of Dortmund, 2003.

[34] V. Selmin, Finite element solution of hyperbolic equations. I. One-dimensional case. *INRIA Research Report* **655** (1987).

[35] V. Selmin, Finite element solution of hyperbolic equations. II. Two-dimensional case. *INRIA Research Report* **708** (1987).

[36] P. K. Sweby, High resolution schemes using flux limiters for hyperbolic conservation laws. *SIAM J. Numer. Anal.* **21** (1984), 995–1011.

[37] S. Turek *et al.*, *FEATFLOW: finite element software for the incompressible Navier-Stokes equations.* User manual, University of Dortmund, 2000. Available at the URL *http://www.featflow.de.*

[38] S. Turek, *Efficient Solvers for Incompressible Flow Problems: An Algorithmic and Computational Approach*, LNCSE 6, Springer, 1999.

[39] S. T. Zalesak, Fully multidimensional flux-corrected transport algorithms for fluids. *J. Comput. Phys.* **31** (1979) 335–362.